Rare Metal Materials and Engineering
Volume 54, Issue 6, June 2025
Available online at www.rmme.ac.cn

Science Press

Cite this article as: Li Chenchen, Ren Xuepeng, Pan Laitao, et al. Inherent Strain Modeling of Residual Stress and Deformation for Laser Powder Bed Fused Artificial Knee Implants Under Different Building Schemes[J]. Rare Metal Materials and Engineering, 2025, 54(06): 1417-1425. DOI: https://doi. org/10.12442/j. issn. 1002-185X.20240247.

ARTICLE

Inherent Strain Modeling of Residual Stress and Deformation for Laser Powder Bed Fused Artificial Knee Implants Under Different Building Schemes

Li Chenchen[1], Ren Xuepeng[1], Pan Laitao[1], Shen Falei[1], Fang Xiaoying[1,2]

[1] School of Mechanical Engineering, Shandong University of Technology, Zibo 255000, China; [2] Institute of Additive Manufacturing, Shandong University of Technology, Zibo 255000, China

Abstract: Through a modified inherent strain model based on the minimum residual stress and deformation, three building schemes with different building postures and support structures were evaluated by finite element analysis. Results demonstrate that according to the principle of reducing the overall height of the building and reducing the support structure with a large tilt angle from the building direction, the residual stress and deformation can be effectively reduced by proper design of building posture and support before laser powder bed melting. Moreover, without the data of thermophysical property variation of Ti-6Al-4V artificial knee implants with temperature, predicting the residual stress and deformation with acceptable accuracy and reduced time cost can be achieved by the inherent strain model.

Key words: residual stress; inherent strain method; titanium alloy; laser powder bed fusion; additive manufacturing

1 Introduction

Laser powder bed fusion (LPBF) has been widely used in aerospace, biomedical, and automotive industries because LPBFed parts have superior performance of complex geometry[1–8]. In LPBF process, metal parts are built layer by layer through the selective melting and rapid solidification of powder, which can be regarded as the formation of numerous microwelds. The fast thermal cycle as well as the localized heat input in the materials tends to generate high residual stress, which can lead to part distortion or even cracking in the final products[9–15].

Residual stresses typically arise from extremely inhomogeneous local thermal distribution after rapid heating and cooling during LPBF. As the thermal stress accumulates due to repeated heating and cooling processes during the whole building operation and reaches the critical strength value, local distortion or even cracks may occur[16–20].

In biomedical applications, Ti-6Al-4V alloy is commonly used as a structural implant material for the human body, which can replace the lost or diseased biological structure of the human body and improve the quality of life[21]. With the aging population, artificial knee replacement surgery is one of the most effective treatments for knee osteoarthritis. Ti-6Al-4V alloy is the most widely used titanium alloy in orthopedics[22]. LPBF technique offers the possibility to customize bone replacements for patients. Reducing the residual stress is a big challenge for manufacturing complex parts, such as artificial knee joint (AKJ) manufactured by LPBF. Optimizing process parameters and building schemes, which involve building posture and support structure, to reduce residual stress is an expensive and time-consuming process via experiments. Alternatively, the finite element model is frequently used to simulate LPBF process and to predict the residual stress distributions[23]. Kundakcioglu et al[24] reported a novel transient thermal analysis approach for additive manufacturing (AM) process simulations of blood

Received date: May 26, 2024
Foundation item: Natural Science Foundation of Shandong Province (ZR2020ME020)
Corresponding author: Fang Xiaoying, Ph. D., Professor, School of Mechanical Engineering, Shandong University of Technology, Zibo 255000, P. R. China, E-mail: fxy@sdut.edu.cn

pump microimpellers for biomedical applications in a powder bed system using a laser heat source. The predicted transient temperature distribution agrees well with the experimental ones. However, the calculation is extremely time-consuming. The real construction process of 2 s takes up to 460 h of calculations. Denlinger et al[25] used thermomechanical simulation to predict the deformation accumulation of an electron beam melted part with a large size on the order of meters. Although the simulation and experimental results show a good agreement with a maximum error of 29%, the process involving 107-layer model took 631 h for computation. To date, the coupled thermomechanical simulations without many simplifications are hardly employed for a real-size part manufactured by LPBF due to the long process time and the large number of time steps, although the model exhibits a high fidelity.

Ueda et al[26] established the inherent strain method for fast estimation of the residual stress and strain of welded parts. Numerous simulation and experimental results have demonstrated the accuracy and effectiveness of this method in predicting residual stress and strain in AM and metal welding processes[27–33] using a linear elastic model instead of the time-consuming thermomechanical model.

Considering that most methods to reduce residual stresses are based on changing process parameters, such as power, scan speed, layer thickness, scan spacing, and scan strategy, few studies have been conducted to reduce residual stresses by changing the build posture and support structure of the complex parts, such as medical implants. In this research, the inherent strain method was employed to predict the residual stress and distortion of AKJ made of Ti-6Al-4V alloy by LPBF process. Firstly, the inherent strain was extracted from the cantilever beam manufactured by LPBF and then applied to the simulation of the artificial knee implant. Secondly, the distributions of residual stress and deformation were predicted for the artificial knee implant built at different postures with different support structures. Finally, the predicted residual stress values were validated with the experimentally measured ones for AKJ built by LPBF process.

2 Experiment

The chemical composition of Ti-6Al-4V metal powder with an average size of approximately 55 μm is listed in Table 1. The corresponding material properties used in the numerical simulation are listed in Table 2.

To determine the inherent strain scaling factor (SSF) used for the simulation of residual stress, the cantilever beam was built on an SLM 125 machine. The dimension of the cantilever beam is shown in Fig. 1a. The teeth-like support structure was adopted to ensure that the overhanging part of the cantilever beam could be prepared with good quality. The optimized LPBF process parameters were used, as listed in Table 3. The substrate was preheated at 200 °C and the high-purity argon gas was used to prevent oxidation during the whole LPBF operation.

Table 1 Composition of Ti-6Al-4V metal powder (wt%)

Al	V	C	Fe	O	N	H	Ti
6.37	3.88	0.01	0.21	0.08	0.01	0.002	Bal.

Table 2 Properties of Ti-6Al-4V alloy used in simulation

Property	Value
Temperature/°C	20
Density/g·cm^{-3}	4.405
Young's modulus/GPa	107
Poisson's ratio	0.323
Yield stress/GPa	1.098

For the practical LPBF process, the cantilever beam was composed of 417 thin layers. To improve the finite element simulation efficiency, the cantilever beam was divided into 25 layers and the thickness of each layer was 0.5 mm. The block element meshing model of the cantilever beam is shown in Fig. 1b. The von Mises yield criterion was selected for the solution method of equivalent stress and strain. The calculation of residual stress and distortion was conducted through element birth and death techniques.

To investigate the influences of the building posture and support structure on the residual stress and deformation of AKJ, three building schemes were proposed, as shown in Fig. 2. The samples of building scheme I and II possess different support structures and the same building posture. The samples of the building schemes II and III possess different building postures and nearly the same supporting structure. The mesh type was hierarchical tetrahedral, which has been proven to be favorable[34] in terms of conforming to the actual geometry of the part, especially in the high curvature region. AKJ models under building schemes I and II were divided into 89 mesh layers and AKJ model under building scheme III was divided into 110 mesh layers. The thickness of each simulation layer was 0.6 mm. The workbench module of the commercial ANSYS software was employed to simulate the

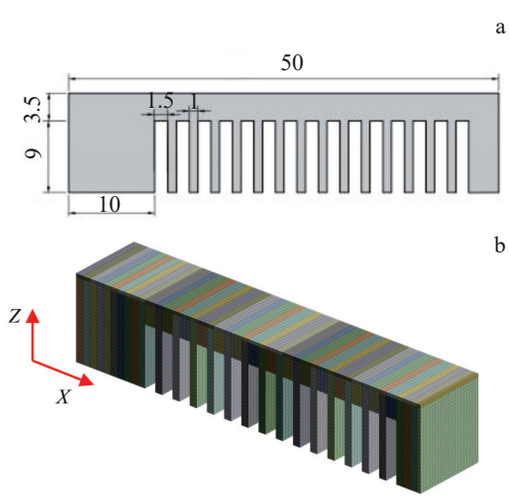

Fig.1 Geometry (a) and meshing (b) appearances of cantilever beam

Table 3 LPBF processing parameters

Parameter	Value
Laser power/W	275
Laser scanning velocity/mm·s^{-1}	1100
Layer thickness/μm	30
Hatching space/μm	120
Laser beam diameter/μm	100

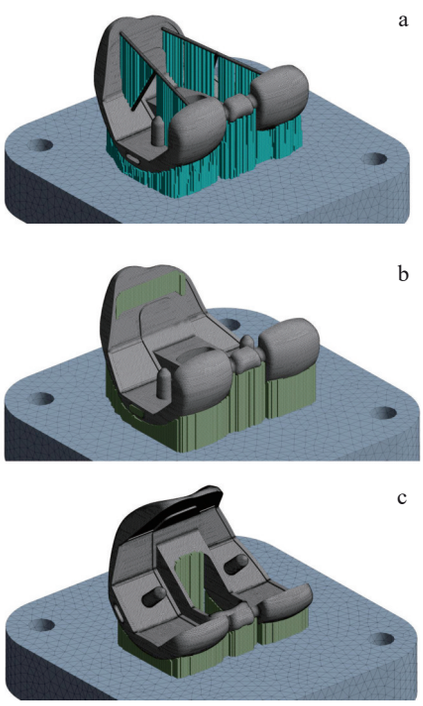

Fig.2 Building scheme I (a), scheme II (b), and scheme III (c) of LPBFed AKJ

stress and strain of LPBFed parts.

To verify the finite element simulation results on the residual stress, 18 locations were randomly selected and used for the residual stress measurement in LPBFed AKJ. The measurements were conducted by X-ray diffraction (XRD) on Stresstech XStress 3000 G2R. The X-rays were generated using a Ti target at 30 kV and 7 mA. Seven ψ (the angle between the examined surface and the diffraction crystal plane) values, including $-45°$, $-35.3°$, $-24.1°$, $0°$, $24.1°$, $35.3°$, and $45°$, were selected for each measurement by the side-inclination method. The diffraction angle, Young's modulus, diffraction crystal plane, and Poisson's ratio were 142°, 110 GPa, {213}, and 0.34, respectively.

3 Finite Element Modeling of LPBF Process

3.1 Inherent strain method

The inherent strain $\varepsilon^{\text{inherent}}$ can be calculated based on Eq.(1), as follows:

$$\varepsilon^{\text{inherent}} = \text{SSF}\frac{\sigma_{\text{yield}}}{E} \tag{1}$$

where σ_{yield} and E represent the yield strength and the elastic modulus of the material, respectively.

SSF is an important factor in quantifying the deformation of samples under different LPBF process conditions. The detailed procedure to determine SSF is shown in Fig.3. Firstly, the displacement d_{exp} was measured when the cantilever beam fabricated by LPBF is removed from the substrate. Then, simulations were performed using the same geometric model and material with the SSF_0 of 1 by default, and the simulated deformation d_{sim} of the model was obtained. Therefore, SSF could be calculated based on Eq.(2), as follows:

$$\text{SSF} = \frac{d_{\text{exp}}}{d_{\text{sim}}}\text{SSF}_0 \tag{2}$$

3.2 Residual stress and strain simulation

The residual stress can be considered to relate to the inherent strain[35]. The inherent strain can be expressed by Eq.(3), as follows:

$$\begin{aligned}\varepsilon^{\text{inherent}} &= \varepsilon^{\text{total}} - \varepsilon^{\text{elastic}} \\ &= \varepsilon^{\text{thermal}} + \varepsilon^{\text{plastic}} + \varepsilon^{\text{phase}} + \varepsilon^{\text{creep}}\end{aligned} \tag{3}$$

$$\{\varepsilon^{\text{total}}\} = \boldsymbol{B}^*\{u\} \tag{4}$$

$$\{\varepsilon^{\text{total}}\} = \{\varepsilon^{\text{elastic}}\} + \{\varepsilon^{\text{inherent}}\} \tag{5}$$

$$\{\varepsilon^{\text{elastic}}\} = \boldsymbol{F}\{\varepsilon^{\text{inherent}}\} \tag{6}$$

$$\{\sigma\} = \boldsymbol{E}\{\varepsilon^{\text{elastic}}\} \tag{7}$$

where $\varepsilon^{\text{total}}$ represents the total strain and can be calculated based on the measured displacement u by Eq.(4); $\boldsymbol{B}$ represents the strain-displacement matrix; $\varepsilon^{\text{thermal}}$ represents the thermal strain; $\varepsilon^{\text{creep}}$ and $\varepsilon^{\text{phase}}$ represent creep strain and phase transformation, respectively; $\varepsilon^{\text{inherent}}$ is equal to plastic strain $\varepsilon^{\text{plastic}}$; σ is residual stress; $\boldsymbol{E}$ and $\boldsymbol{F}$ in Eq. (6) and Eq. (7) represent the stress-strain matrix and strain coefficient matrix, respectively.

Considering that $\varepsilon^{\text{thermal}}$ disappears with the decrease in temperature, creep strain $\varepsilon^{\text{creep}}$ and phase transformation $\varepsilon^{\text{phase}}$ are negligible, compared with plastic deformation. The

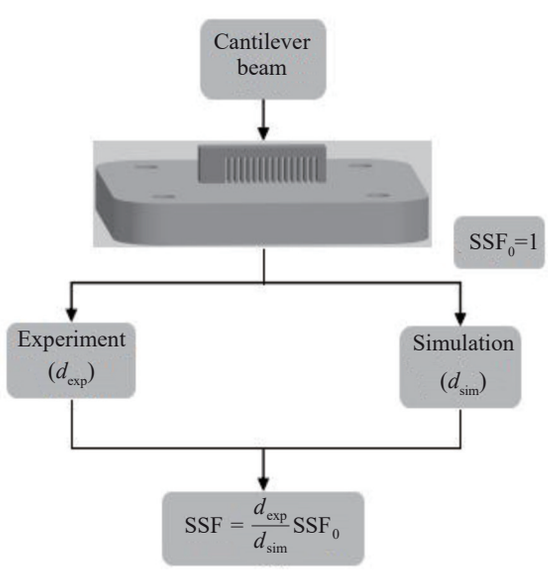

Fig.3 SSF determination process

relationship between ε^{total} and $\varepsilon^{inherent}$ can be simplified as Eq.(5). The relationship among the residual stress σ, inherent strain $\varepsilon^{inherent}$, and elastic strain $\varepsilon^{elastic}$ can be derived from Eq.(6–7).

3.3 Layer-by-layer activation

The LPBFed part is typically formed by melting and cooling layer by layer. Each layer can be regarded as a basic unit generating an inherent strain for LPBF simulation. The inherent strain was applied to each mesh element to calculate the deformation and stress while ignoring the transient process of LPBF. The deformation was introduced into the body by layer-by-layer activation of inherent strain. The first layer on the substrate was activated to calculate the stress and deformation using the inherent strain while the rest layers were deactivated. Then, the next layer was activated and the same operation was repeated until the entire layers of the part were completed.

4 Results and Discussion

4.1 Experiment results of cantilever beam

The cantilever beam manufactured by LPBF is shown in Fig. 4a. The necking shrinkage can be observed near the interface between the overhanging beam and the teeth-like support, as indicated by the white arrow in Fig. 4a. This necking shrinkage should result from the sudden change of the cross-sectional area from the overhanging beam to the teeth-like support. In addition, an observable warping deformation occurs when the cantilever beam part with the teeth-like support is separated from the substrate with the left part still being fixed on the substrate, as shown in Fig. 4a. The maximum warping on the right end of the cantilever beam is measured to be 1.25 mm.

The simulated deformation result using an initial SSF_0 of 1 for the cantilever beam is shown in Fig. 4b. The maximum warping on the right end of the cantilever beam is calculated to be 5.32 mm. Therefore, SSF under the current LPBF process parameters can be derived as 0.235, which is in turn input to the simulation model to predict the deformation. It is clear that the newly simulated deformation result (Fig. 4c) is quite consistent with the experimental one (Fig. 4a). As reported in Ref. [36 – 37], the cantilever beam is a common benchmark model to verify the simulation accuracy of the LPBF process. To further substantiate this phenomenon in this research, the warping deformation of the 10 locations along the cantilever beam was examined and compared with the simulated ones. For each location, the warping value is averaged over 10 measurements. As shown in Fig. 5, the simulation results are in good agreement with the experimental ones, which indicates that the model is reliable for the prediction of deformation and even residual stress of LPBFed parts.

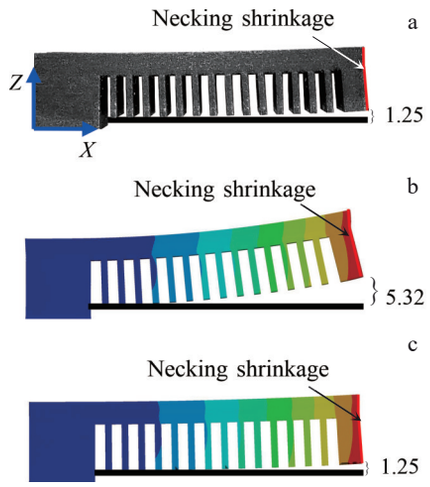

Fig.4 Deformation of cantilever beam after separation from substrate: (a) real deformation of cantilever beam; (b) simulated deformation of cantilever beam with SSF_0=1; (c) simulated deformation of cantilever beam with SSF_{new}= 0.235

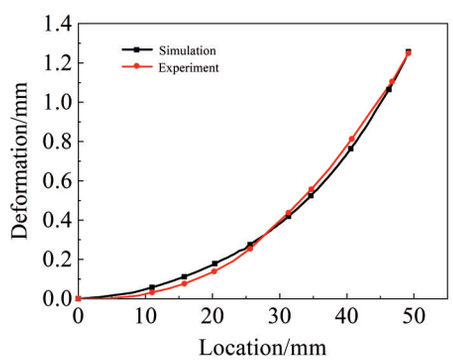

Fig.5 Comparison of experiment and simulation results of deformation along the top centerline of cantilever beam

4.2 Simulation results of AKJ

4.2.1 Deformation distribution

Fig.6 shows the deformation distribution of AKJ with (Fig.6a –6c) and without (Fig.6d–6f) support structures under different building schemes. It can be seen that the maximum deformation occurs in the support structure, the transitional area of a differently oriented cross-section, and the area near the outer side, as indicated by black arrows in Fig. 6. These locations usually involve a large cooling rate and therefore exhibit high residual stress and deformation. Secondly, AKJ of building scheme Ⅲ possesses the minimum deformation while that of building scheme Ⅰ exhibits the maximum deformation with the support structure. Thirdly, after the support structure is removed, the maximum deformation decreases for AKJ of building scheme Ⅰ and Ⅱ, whereas the deformation distribution of AKJ of building scheme Ⅲ does not exhibit any change. It is suggested that the support structure of the building scheme Ⅲ does not have many effects on stress release. It should be ascribed to its tall building posture, which weakens the benefits of the support structure. By comparison, the supporting structure of building scheme Ⅱ is the most effective in reducing the deformation of AKJ, although its support structure seems simpler than that of building scheme Ⅰ, where an additional upper support structure denoted by red arrow in

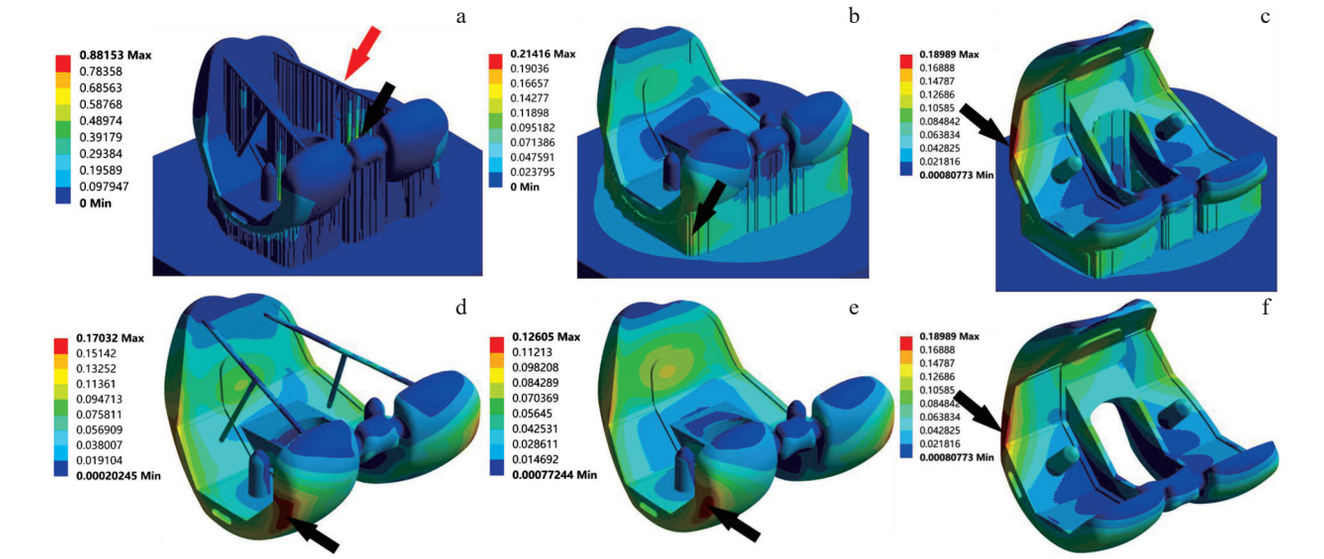

Fig.6 Deformation distributions of AKJs with (a–c) and without (d–f) support structures under building scheme Ⅰ (a, d), scheme Ⅱ (b, e), and scheme Ⅲ (c, f)

Fig. 6a is designed. This upper support structure of building scheme Ⅰ has a large tilt angle with the building direction and may introduce residual stress or deformation into AKJ due to excessive constraints, compared with that of building scheme Ⅱ. In addition, the distributions of the deformation components along the *X, Y,* and *Z* directions are presented in Fig.7. It is obvious that the deformation along *Z* direction, namely the building direction, is typically larger than that along *X* and *Y* directions in all building schemes. It is suggested that the stress concentration is more severe along the building direction (*Z*) than the scanning plane (*XY*) due to the inherent layer-by-layer building mode during LPBF process.

4.2.2 Residual stress distribution

Fig. 8 shows the residual stress distributions of AKJ with (Fig. 8a–8c) and without (Fig. 8d–8f) support structures under different building schemes. It is found that nearly no change occurs in the residual stress distribution with the deformation varies, especially for AKJ with building scheme Ⅰ and Ⅱ when the support structure is removed for the samples. The relatively high deformation induced during LPBF (Fig. 6) releases most of the residual stress in the support structure after the support structure is removed, and therefore nearly no change occurs in residual stress distribution. In addition, AKJ of building scheme Ⅲ possesses the highest residual stress whereas AKJ of building scheme Ⅰ exhibits the lowest residual stress. AKJ of building scheme Ⅱ exhibits a little higher residual stress than AKJ of building scheme Ⅰ. The maximum deformation and maximum stress under different schemes are summarized in Table 4.

It should be noted that the maximum stress typically occurs at the outer surfaces[38–39] and the zones with the sudden change in cross-sectional area for AKJs of all three schemes, as indicated in Fig. 8. To further compare the residual stress distribution, the variation of residual stress on the same segmented line ACB, as shown in Fig. 9a, is presented in Fig. 10. It is obvious that the maximum residual stress occurs at the intersecting point C in all three schemes. AKJ of building scheme Ⅲ has the highest residual stress of 725 MPa. It can also be found that asymmetrical stress distribution exists for AKJ of building scheme Ⅰ and Ⅱ and symmetrical stress distribution exists for AKJ of building scheme Ⅲ along line ACB. This result is related to their locations or heights in terms of the building direction. The residual stress distribution on an equivalent inner profile for AKJs of different building schemes is shown in Fig. 11. The stress typically accumulates along the building direction, which is particularly obvious at the large height level of the part. The overall building heights of building scheme Ⅰ and Ⅱ are equivalent and smaller than the building height of building scheme Ⅲ, which costs more building time and leads to higher residual stress. Therefore, building scheme Ⅲ is the most unfavorable for LPBFed AKJ. After the support structure is removed, the minimum strain and moderate stress occur in AKJ of building scheme Ⅱ. Thus, building scheme Ⅱ can be considered as optimal selection in terms of building posture and support structure for producing AKJ by LPBF process. The residual stress components along *X*, *Y*, and *Z* directions on an inner profile indicated by A-A plane in Fig. 9b for AKJ of building scheme Ⅱ are shown in Fig. 12. It can be seen that the stress component along *Z* direction is far larger than that along *X* or *Y* directions. Thus, decreasing the building height as much as possible is a priority criterion for selecting the building posture of a complex-shaped part.

4.3 Experiment verification on residual stress and deformation

18 locations were randomly selected for residual stress evaluation in the outer side of AKJ of building scheme Ⅱ, as shown in Fig. 13, using Stresstech XStress 3000 G2R. The experimental results are compared with the simulated ones, as shown in Fig. 14. It can be seen that the simulated values have

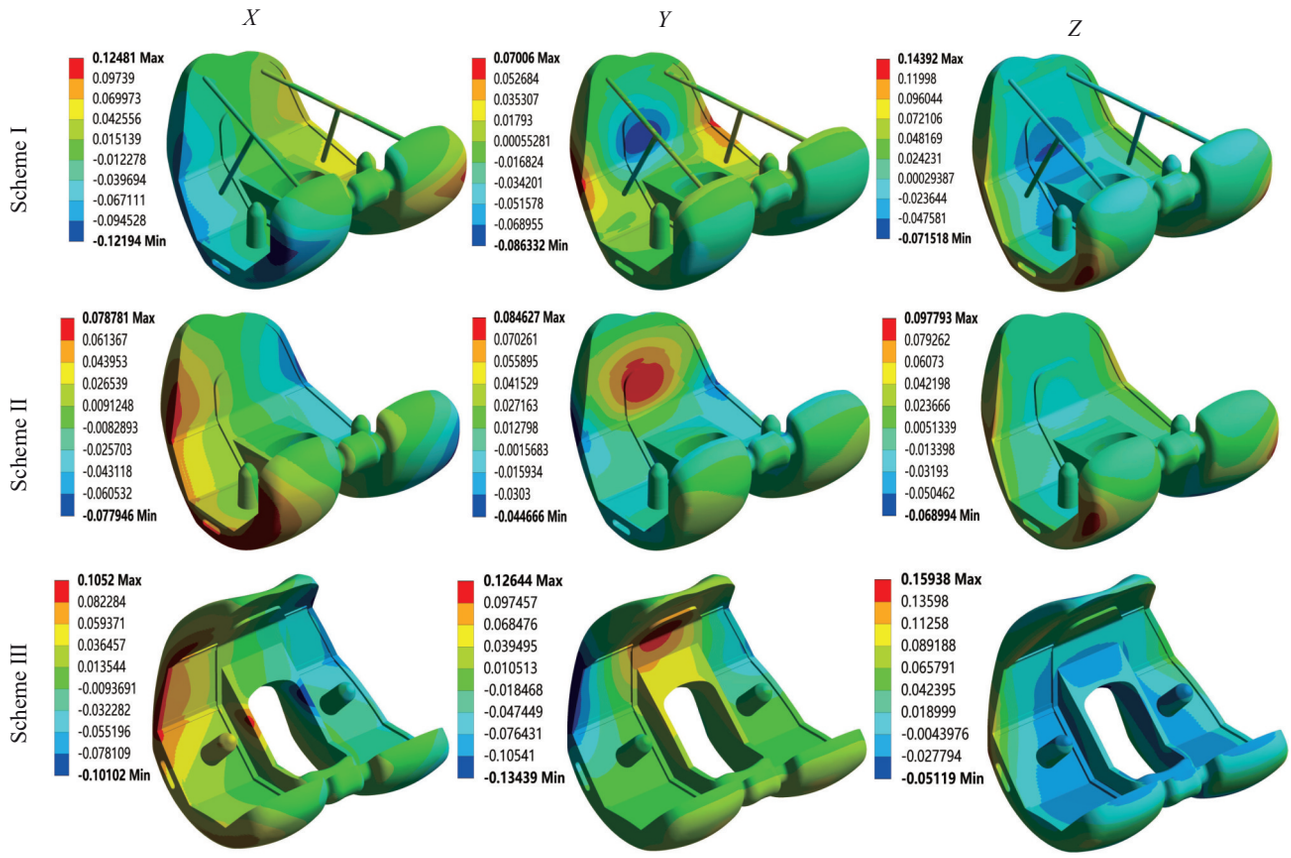

Fig.7 Deformation distributions along different directions of AKJ under different building schemes

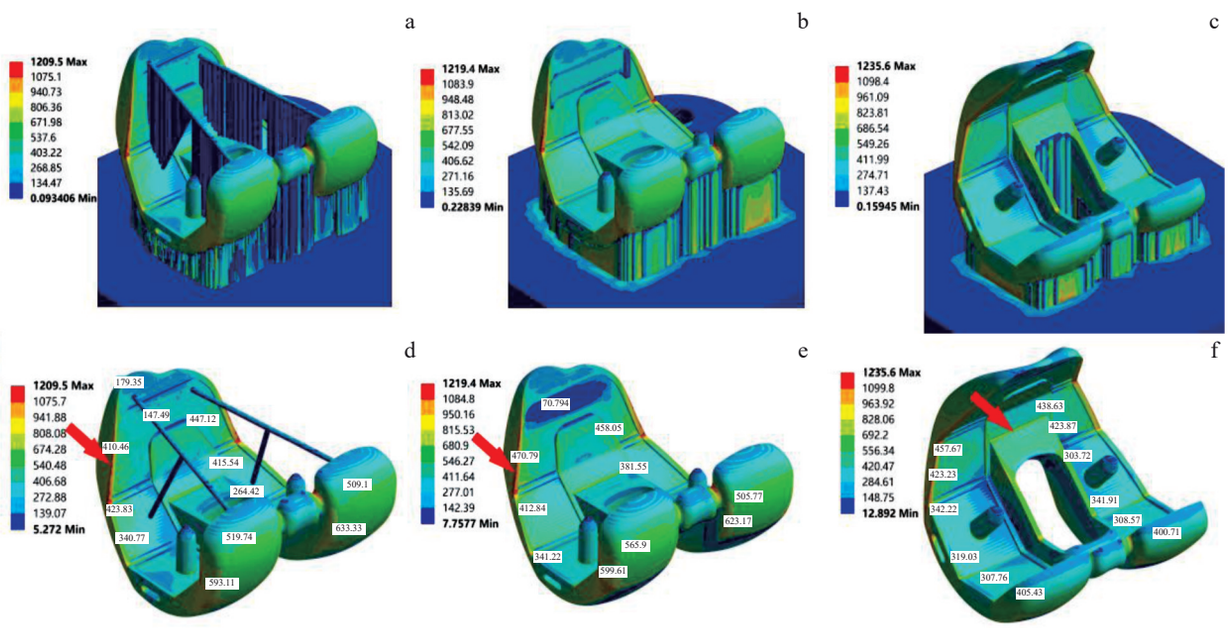

Fig.8 Residual stress distributions of AKJ with (a–c) and without (d–f) support structure under building scheme (a, d), scheme Ⅱ (b, e), and scheme Ⅲ (c, f)

a good agreement with the experimental ones and the deviations are within 20%, indicating that the modified inherent strain model has a great potential to predict the residual stress and deformation distribution of LPBFed parts, particualrly when the functions of thermophysical properties with temperature of materials are unknown. Besides, it can be

Table 4 Maximum strain and maximum stress of AKJ under different building schemes

Building scheme	Maximum strain/mm	Maximum stress/MPa
Ⅰ	0.17	1209.5
Ⅱ	0.13	1219.4
Ⅲ	0.19	1235.6

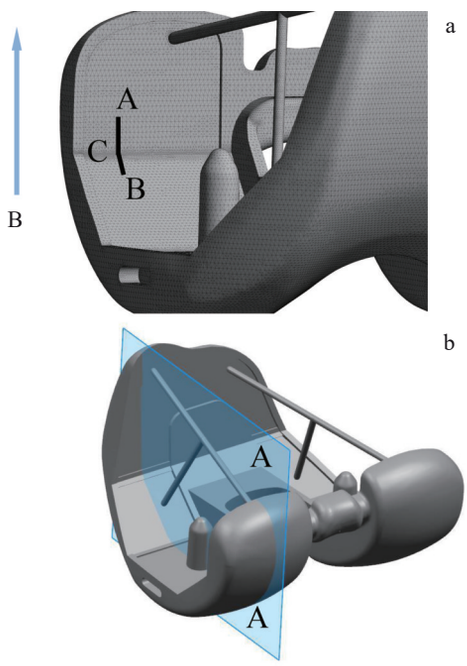

Fig.9 Selected path of line ACB (a) and A-A cross-sectional configuration (b) in AKJ

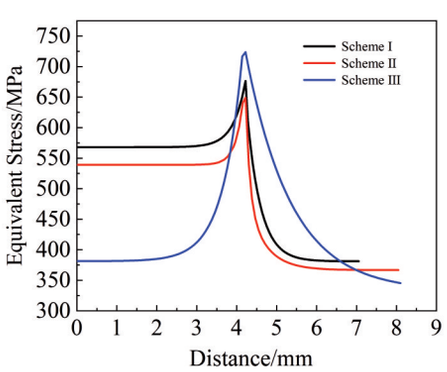

Fig.10 Residual stress variations along line ACB in Fig. 9a of AKJs of different building schemes

concluded that appropriate building posture and support structure designs prior to LPBF can effectively reduce the residual stress and deformation according to the principle of reducing the overall height of the building and reducing the

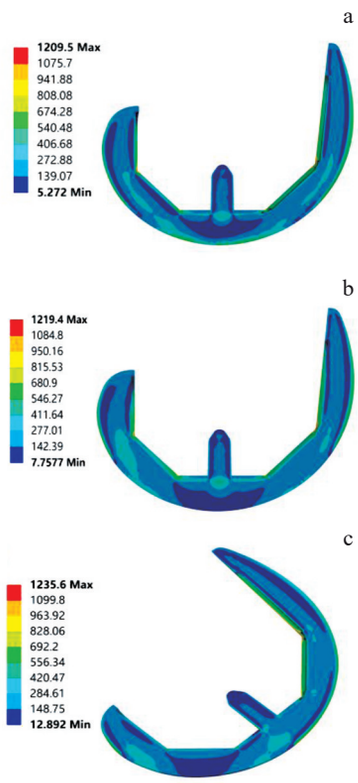

Fig.11 Residual stress distributions in AKJs of building scheme Ⅰ (a), building scheme Ⅱ (b), and building scheme Ⅲ (c)

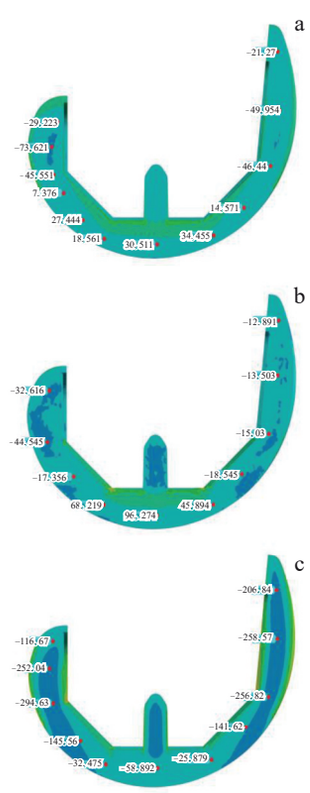

Fig.12 Stress distributions along *X* direction (a), *Y* direction (b), and *Z* direction (c) of A-A cross-section in Fig. 9b of AKL of building scheme Ⅱ

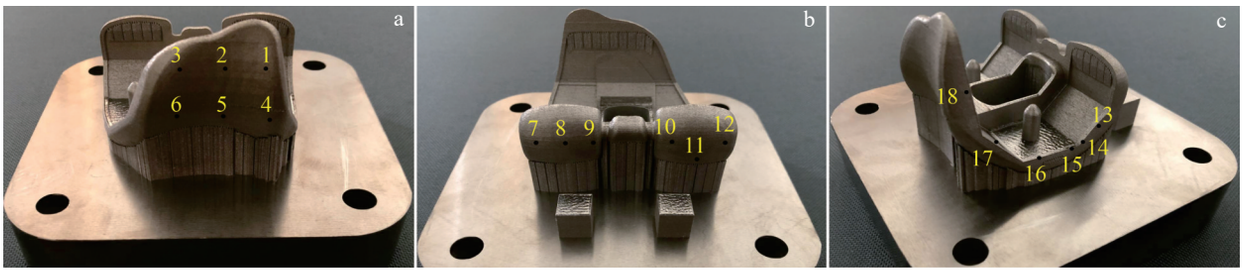

Fig.13 Selected points for residual stress measurement of AKJ of building scheme Ⅱ: (a) points 1–6, (b) points 7–12, and (c) points 13–18

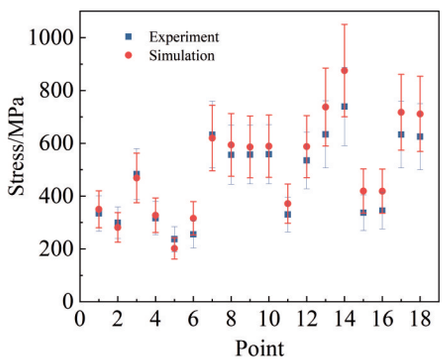

Fig. 14 Comparison between experimental and simulated results of residual stress of 18 points of AKJ of building scheme Ⅱ

support structure with a large tilt angle from the building direction.

5 Conclusions

1) The maximum stress is typically on the outer surface or locations with the sudden change of cross-sectional area, which is more obvious when the building height increases.

2) Predicting the residual stress and deformation with acceptable accuracy can be realized using the modified inherent method for complex-shaped LPBFed parts without the thermophysical properties of materials at elevated temperatures.

3) Appropriate building posture and support structure designs prior to LPBF can effectively reduce the residual stress and deformation according to the principle of reducing the overall height of the building and reducing the support structure with a large tilt angle from the building direction.

References

1 Wang X, Zhang P, Ludwick S *et al*. *Additive Manufacturing*[J], 2018, 20: 189

2 Zhang P, Toman J, Yu Y *et al*. *Journal of Manufacturing Science and Engineering*[J], 2015, 137: 021004

3 Bhavar V, Kattir P, Patil V *et al*. *4th International Conference and Exhibition on Additive Manufacturing Technology*[C]. Bangalore: EFESTO, 2014: 1

4 Khairallah S A, Anderson A T, Rubenchik A *et al*. *Acta Mater*[J], 2016, 108: 36

5 Mower T M, Long M J. *Materials Science and Engineering A*[J], 2016, 651: 198

6 Li C, Fu C H, Guo Y B *et al*. *Procedia Manufacturing*[J], 2015, 1: 355

7 Gu D D, Meiners W, Wissenbach K *et al*. *International Materials Reviews*[J], 2013, 57: 133

8 Cheng L, Zhang P, Biyikli E *et al*. *Rapid Prototyping Journal*[J], 2017, 23(4): 660

9 Zhao X, Lin X, Chen J *et al*. *Materials Science and Engineering A*[J], 2009, 504: 129

10 Shiomi M, Osakada K, Nakamura K. *CIRP Annals*[J], 2004, 53(1): 195

11 Lewis G K, Schlienger E. *Materials and Design*[J], 2000, 21(4): 417

12 Mercelis P, Kruth J P. *Rapid Prototyping Journal*[J], 2006, 12(5): 254

13 DebRoy T, Wei H L, Zuback J S *et al*. *Progress in Materials Science*[J], 2018, 92: 112

14 Kempen K, Thijs L, Vrancken B *et al*. *24th International Solid Freeform Fabrication Symposium*[C]. Austin: Laboratory for Freeform Fabrication, 2013: 131

15 Denlinger E R, Heigel J C, Michaleris P *et al*. *Journal of Materials Processing Technology*[J], 2015, 215: 123

16 Takezawa A, Chen Q, Liang X *et al*. *Computer Methods in Applied Mechanics and Engineering*[J], 2020, 370: 113231

17 Yasa E, Deckers J, Craeghs T *et al*. *20th International Solid Freeform Fabrication Symposium*[C]. Austin: Laboratory for Freeform Fabrication, 2009: 180

18 Beal V E, Erasenthiran P, Hopkinson N *et al*. *International Journal of Production Research*[J], 2008, 46(1): 217

19 Mercelis P, Kruth J P. *Rapid Prototyping Journal*[J], 2006, 12(5): 254

20 Wu A S, Brown D W, Kumar M *et al*. *Metallurgical and Materials Transactions A*[J], 2014, 45: 6260

21 Laleh M, Sadeghi E, Revilla R I *et al*. *Progress in Materials Science*[J], 2023, 133: 101051

22 Zhang Yongdi, Wang Congyu, Wang Congwei *et al*. *Rare Metal Materials and Engineering*[J], 2022, 51(5): 1690 (in Chinese)

23 Vastola G, Zhang G, Pei Q X *et al*. *Additive Manufacturing*[J],

2016, 12: 231
24 Kundakcioglu E, Lazoglu I, Rawal S. *The International Journal of Advanced Manufacturing Technology*[J], 2015, 85: 493
25 Denlinger E R, Irwin J, Michaleris P. *Journal of Manufacturing Science and Engineering*[J], 2014, 136: 061007
26 Ueda Y, Fukuda K. *Journal of Engineering Materials & Technology*[J], 1989, 111(1): 1
27 Alvarez P, Ecenarro J, Setien I *et al*. *International Journal of Engineering Research & Science*[J], 2016, 2(10): 39
28 Afazov S, Denmark W A D, Toralles B L *et al*. *Additive Manufacturing*[J], 2017, 17: 15
29 Peter N, Pitts Z, Thompson S *et al*. *Additive Manufacturing*[J], 2020, 36: 101531
30 Tsai C L, Cheng W T, Lee H T. *Modeling Strategy for Control of Welding-Induced Distortion*[R]. Warrendale: Minerals, Metals and Materials Society, 1995
31 Ueda Y, Murakawa H, Nakacho K *et al*. *Transactions of JWRI* [J], 1995, 24: 73
32 Murakawa H. *Mathematical Modelling of Weld Phenomena*[M]. Boca Raton: CRC Press, 1998: 4
33 Keller N, Ploshikhin V. *25th International Solid Freeform Fabrication Symposium*[C]. Austin: Laboratory for Freeform Fabrication, 2014: 1229
34 Weber S, Montero J, Bleckmann M *et al*. *Procedia CIRP*[J], 2020, 91: 522
35 Yuan M G, Ueda Y. *Journal of Engineering Materials and Technology*[J], 1996, 118: 229
36 Setien I, Chiumenti M S, Veen V D *et al*. *Computers & Mathematics with Applications*[J], 2019, 78: 2282
37 Siewert M, Neugebauer F, Epp J *et al*. *Computers & Mathematics with Applications*[J], 2019, 78: 2407
38 Sirin T B, Kaynak Y. *Procedia CIRP*[J], 2021, 99: 330
39 Bagg S D, Sochalski-Kolbus L M, Bunn J R. *2016 Summer Topical Meeting: Dimensional Accuracy and Surface Finish in Additive Manufacturing*[C]. Raleigh: American Society of Precision Engineering, 2016

激光粉末床熔融人工膝关节植入物在不同构建方案下残余应力和变形的固有应变建模

李晨晨[1]，任雪彭[1]，潘来涛[1]，申发磊[1]，方晓英[1,2]
(1. 山东理工大学 机械工程学院，山东 淄博 255000)
(2. 山东理工大学 增材制造研究所，山东 淄博 255000)

摘　要：采用基于最小残余应力和变形的修正固有应变模型，对具有不同打印建造姿态和支撑结构的3种打印建造方案进行了有限元分析。结果表明，以降低打印建造整体高度和减少与打印建造方向倾斜角较大的支撑结构为准则，在进行激光粉末床熔融前进行适当的打印建造姿态和支撑设计，可以有效地减小残余应力和变形。此外，在不知道Ti-6Al-4V人工膝关节热物性随温度变化的情况下，利用固有应变模型预测其残余应力和变形，可以获得较好的精度并节约时间成本。

关键词：残余应力；固有应变法；钛合金；激光粉末床熔融；增材制造

作者简介：李晨晨，女，2000年生，硕士生，山东理工大学机械工程学院，山东 淄博 255000，E-mail：lichenchen1129@163.com